GEOMICROBIOLOGY JOURNAL
2022, VOL. 39, NO. 2, 148–154
https://doi.org/10.1080/01490451.2021.2020936

Compressive Strength of MICP-Treated Silica Sand with Different Particle Morphologies and Gradings

Chenpeng Song[a,b,c], Chaoyi Wang[d], Derek Elsworth[b], and Sheng Zhi[b]

[a]Key Laboratory of Hydraulic and Waterway Engineering of the Ministry of Education, Chongqing Jiaotong University, Chongqing, China; [b]Department of Energy and Mineral Engineering, Geosciences, EMS Energy Institute, G3 Center, Pennsylvania State University, University Park, PA, USA; [c]State Key Laboratory Cultivation Base for Gas Geology and Gas Control, Henan Polytechnic University, Jiaozuo, China; [d]Department of Geoscience, University of Calgary, Calgary, Canada

ABSTRACT

Microbially-induced calcium carbonate precipitation (MICP) can enhance the stiffness and bulk strength of sand aggregates *via* calcium carbonate cementation. This study explores the mechanical strength of silica sand aggregates with different particle morphologies and sizes following MICP treatment. Specifically, unconfined uniaxial compressive strength (UCS) of MICP-treated spherical, near-spherical, and angular aggregates are measured for four separate size fractions (18–25, 25–40, 40–60, and 60–80 mesh). Scanning electron microscope (SEM) imaging is performed on post-treatment samples to investigate the difference in cementation morphology and failure mechanisms. The experimental results indicate: (1) given identical cycles of MICP treatment, the UCS of treated spherical and near-spherical sands peaks at 25–40 mesh particle size, while the treated angular sands show increasing UCS with decreasing particle size; (2) spherical sands have the highest calcium carbonate ($CaCO_3$) content given identical MICP cycles; and (3) higher post-treatment $CaCO_3$ content does not correlate to higher UCS—implying that the distribution and morphology of $CaCO_3$ precipitation exert crucial control. SEM analysis shows that $CaCO_3$ fully encapsulates spherical sand particles uniformly, forming point contact bonds. In contrast, $CaCO_3$ precipitations show a patchy distribution on near-spherical and angular sand grain surfaces. Unlike treated spherical sands, treated near-spherical sands feature a mixture of point and planar contact bonds while treated angular sands feature predominantly planar contact bonds. Planar contact bonds provide a larger effective cementation area between sand particles and thus result in higher bonding strength. The particle morphology and resultant inter-particle bonding morphology help reconcile higher ensemble UCS with lower $CaCO_3$ content of treated angular sands.

ARTICLE HISTORY
Received 16 November 2020
Accepted 16 December 2021

KEYWORDS
MICP; microbial cementation; particle morphology; cementation mechanism; uniaxial compressive strength

Introduction

Biomineralization is a biochemical process by which microorganisms synthesize minerals by the mediation of biomacromolecules, including biologically induced mineralization and biologically controlled mineralization (Song and Liu 2020; Wu et al. 2019). *Sporosarcina pasteurii*, formerly *Bacillus pasteurii*, is a nitrogen-circulating ureolytic bacterium that is a well-known microorganism capable of inducing calcium carbonate precipitations. This microorganism can hydrolyze urea (carbamide) into carbonate and ammonium through the secretion of a urease enzyme during its metabolism. This microbially-mediated ureolysis can induce calcium carbonate precipitates under Ca^{2+}-rich environment (Song and Elsworth 2018). Ureolysis-driven calcium carbonate precipitation by *Sporosarcina pasteurii* has attracted considerable attention and is implemented as bio-cement grouting for many geotechnical applications, including soil stabilization, sideslip treatment, and ground improvement (DeJong et al. 2006; Liu et al. 2020; Mortensen and Dejong 2011; Salifu et al. 2016). Effective microbially-induced carbonate precipitation (MICP) requires the optimization of the grouting strategy, grouting rates, reagent concentrations, and retention duration (Al Qabany et al. 2012; Mortensen et al. 2011).

Ottawa sand is natural near-spherical silica sand mined from Ottawa, Illinois area, USA (Imseeh et al. 2020) which is commonly regarded as a standard control granular media to inspect the microscopic behavior and the efficacy of MICP (Cardoso et al. 2020; Choi et al. 2019; DeJong et al. 2006; Mortensen and Dejong 2011; Peng and Liu 2019; Song et al. 2020; Song and Elsworth 2020; Wen et al. 2019). Triaxial test results on MICP treated Ottawa sand, and coarse angular sand indicates an increase in shear strength with larger angularity and smaller particle sizes (Nafisi et al. 2018). Other studies use mixtures of coarse sand (particle size ranging from 2.36 to 16.0 mm) and fine sand (particle size ranging from 0.075 to 9.5 mm) indicates that a 75–25% coarse to fine ratio achieves the highest uniaxial compressive strength after MICP-grouting (Mahawish et al. 2018). However, few studies so far have discussed the correlation

CONTACT Chaoyi Wang chaoyi.wang1@ucalgary.ca Department of Geoscience, University of Calgary, Calgary, AB, T2N1N4, Canada

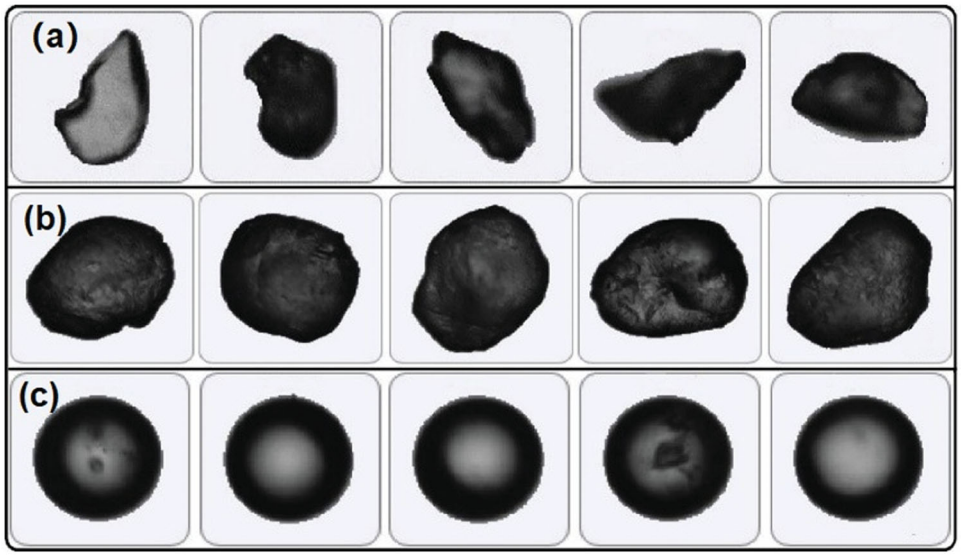

Figure 1. Representative two-dimension projections of sand particles: (a) crushed Ottawa sand (angular); (b) Ottawa sand (near-spherical); (c) artificial silica sand (spherical).

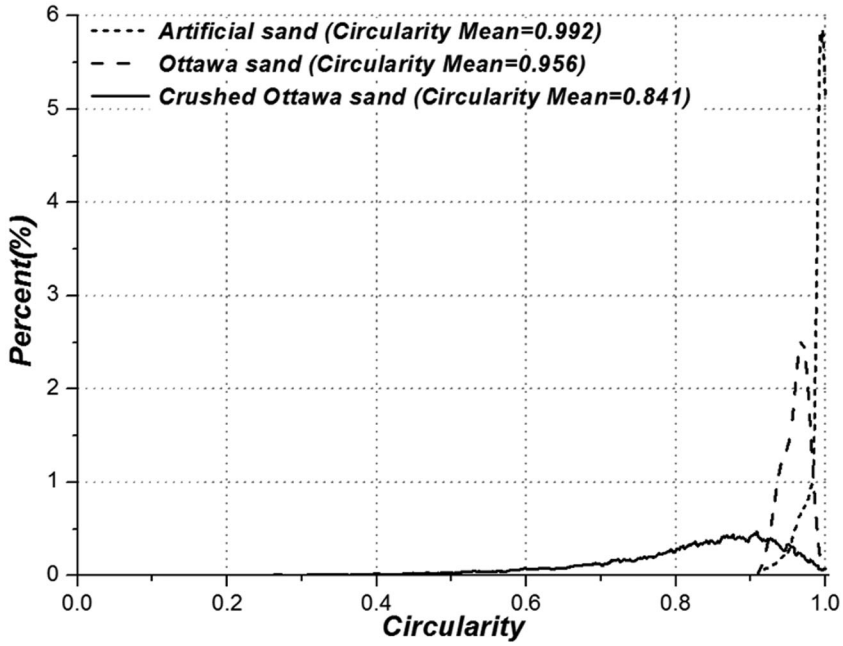

Figure 2. Distributions of sand particle circularity calculated from 2D projection images.

between particle morphology, size, and their influences on MICP treatment cementation mechanisms, especially using spherical particles as control.

This study explores the influences of particle morphology and size grading on the ensemble mechanical strength and microscopic cementation mechanisms of MICP-treated silica sands. Three types of silica sand aggregates are used in this study for MICP-grouting, namely, crushed Ottawa sand (angular), Ottawa sand (near-spherical), and artificial silica sand (spherical). Each type of sand is sieved in four size fractions (18–25, 25–40, 40–60, and 60–80 mesh). The ensemble strength and cementation mechanism of the treated samples are examined through uniaxial compressive strength (UCS) tests and scanning electron microscopy (SEM) imaging.

Materials and methods

Silica sand characterizations

Three types of silica sand with significant differences in particle shape are used for the MICP-grouting in this study. Specifically, crushed Ottawa sand, Ottawa sand, and spherical silica sand, with particle shapes as angular, near-spherical and spherical, respectively. The morphologies of the sand particles are quantitatively characterized by image analysis performed using the Malvern Morphologi® G3 instrument. The representative two-dimension projections of the sand particles are shown in Figure 1. The statistical distributions of the particle circularity calculated from the 2D projection images are shown in Figure 2. Circularity is defined as the closeness to a perfect circle. It is usually

expressed as the ratio of the circumference of a circle with an equivalent area to the actual circumference of the particle 2D projection, ranging from 0 to 1. The more circular the particle is, the closer the circularity is to 1, the more rough-edged or elongated the particle is, the lower the circularity (Ulusoy and Kursun 2011).

Each type of sand is sieved into four size fractions: 18–25 mesh (1.00–0.85 mm), 25–40 mesh (0.85–0.425 mm), 40–60 mesh (0.425–0.250 mm), and 60–80 mesh (0.250–0.180 mm). The prepared materials are thoroughly washed in an HCl solution (5 mol/L) to remove acid-soluble impurities. After the acid wash, the materials are rinsed with purified water and air-dried. The porosity of sand packing for each size fraction is measured by helium porosimetry (the sand sample is carefully vibrated for 1 min under a 100 g weight in the measuring chamber before porosimetry testing, the same procedure is applied to the sand columns prepared for MICP-grouting). Measured data indicates that porosity increases slightly as the circularity decreases (Table 1).

Bacterial culture

Sporosarcina Pasteurii (ATCC 11859) is used for ureolysis-driven MICP. The freeze-dried strain is activated first and then incubated in the ammonium-yeast extract media [10 g ammonium sulfate, 20 g yeast extract, and 0.13 M tris aminomethane buffer (pH = 9.0)] at 30 °C on an oscillator kept at 200 rpm for 36–48 h. The bacterial culture solution is harvested when the biomass reaches OD_{600} = 1.2–1.6. A large batch of the bacterial culture solution is reserved at 4 °C. A sufficient portion of the solution is retrieved from the batch for each MICP-grouting.

Table 1. Sample porosity when packed.

Sand aggregate types	18–25 Mesh	25–40 Mesh	40–60 Mesh	60–80 Mesh
Artificial silica sand	0.379	0.386	0.383	0.385
Ottawa sand	0.392	0.382	0.391	0.397
Crushed Ottawa sand	0.393	0.416	0.418	0.401

Experimental apparatus and strategy for MICP-grouting

The experimental setup for MICP-grouting is illustrated in Figure 3. The sand aggregates are prepared in a PVC tube (6 in/150 mm in length and 1 in/25 mm in inner diameter). The sample preparation procedure for the sand column is the same as that for the porosity measurement. Both ends of the sand column are equipped with a highly-permeable buffer layer to distribute the solutions through the column evenly. The MICP-grouting solutions are injected into the sand column from the bottom of the sample by a micro-syringe pump.

MICP-grouting solutions include the bacterial suspension, fixation solution (0.05 mol/L $CaCl_2$ solution), and nutrient solution (a mixed solution of 1.0 mol/L carbamide and 1.0 mol/L $CaCl_2$). The solutions are injected into the sand column in sequence. The fixation solution contains calcium ions to promote bacteria flocculation and adhesion to the particle surfaces (Song et al. 2020). A typical MICP-grouting cycle in this study is elaborated in Figure 4.

It is worth noting that the purpose of step (e) is to promote uniform distribution of $CaCO_3$ precipitation in the column. A comparison of the increasing grouting cycles is achieved by conducting six, eight, then 10 injection cycles to individual samples from the three types of sands. After MICP-grouting, the sand column is oven-dried for 24 h and trimmed into a standard shape (2 in/5.08 cm in height and 1 in/2.54 cm in diameter in the center of the original core, the ends of the sample are trimmed) for unconfined uniaxial compressive strength (UCS) tests.

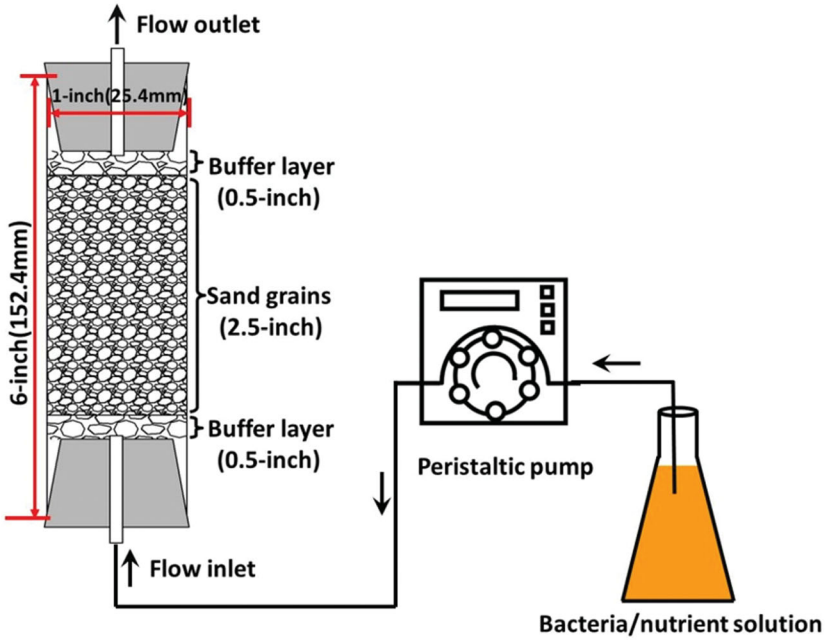

Figure 3. Schematic of the experimental apparatus.

Experimental results

Evolution of uniaxial compressive strength

Correlations between UCS and MICP-grouting cycles (a total of 100 ml nutrient solution is injected into the samples in a single MICP-grouting cycle) for three types of sands are shown in Figures 5(a–c), respectively. Overall, UCS increases with the nutrient injection volume for all test materials. Specifically, the MICP treated Ottawa sand (near-spherical,

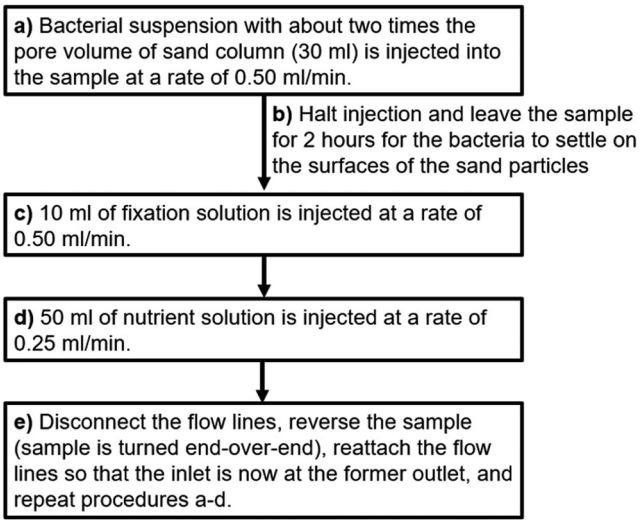

Figure 4. A typical MICP-grouting procedure.

Figure 5(b)) shows the smallest increase in UCS with more grouting cycles compared to the other two materials. The 60–80 mesh crushed Ottawa sand (angular, Figure 5(c)) shows the largest UCS (5.21 MPa). The MICP treated artificial silica sand (spherical) shows a similar increasing trend in UCS as Ottawa sand (near-spherical).

Despite the monotonic increase of UCS with grouting cycles, UCS does not increase monotonically with a decrease in particle sizes in all test materials. The UCS values are plotted against particle sizes in Figures 5(d–f). The UCS of treated artificial silica sand (spherical) and treated Ottawa sand (near-spherical) reaches the maximum for 25–40 mesh particle size and decreases to the minimum for 60–80 mesh particle size. Crushed Ottawa sand (angular), on the contrary, exhibits increases in UCS with decreases in particle sizes, which is consistent with previous laboratory observations on similar materials (Mahawish et al. 2018; Nafisi et al. 2018).

Post-treatment calcium carbonate content

Following the UCS tests, the $CaCO_3$ contents of the treated samples are measured by soaking fragments of the specimen into 5.0 mol/L Hydrochloric acid (HCl) solution for over 24 h to remove $CaCO_3$ precipitation fully. After the acid bath, the samples are washed with purified water and oven-dried. The $CaCO_3$ content is expressed as the ratio of the weight difference pre and post-HCl bath ($CaCO_3$) to the dry weight of residuals (sand aggregates) post-HCl bath. The $CaCO_3$ contents are listed in Table 2. Overall, $CaCO_3$ contents increase with MICP-grouting cycles. Specifically, the $CaCO_3$ content of the artificial silica sand (spherical) is significantly higher than the other two types given identical MICP-grouting cycles. UCS values are plotted against $CaCO_3$ contents for three types of sands in Figure 6. It can be seen that treated artificial silica sands (spherical) feature the highest $CaCO_3$ content given the same grouting cycles compared to the other two types of treated sands. However, treated artificial silica sands (spherical) do not consistently show higher UCS, especially for the particle size of 40–60 and 60–80 mesh. Observing Figures 6(a–d), the crushed Ottawa sand (angular) indicates a larger gain in UCS, given similar or less $CaCO_3$ content compared to the other two types. Specifically, treated crushed Ottawa sand (angular) returns the highest UCS (5.21 MPa) among the three after 10 cycles of MICP-grouting for 60–80 mesh particle size. However, its $CaCO_3$ content (16.3%) is much lower than the treated artificial silica sand (27.3%), which only returns a UCS of 1.32 MPa. This observation can be reconciled by examining the distribution of $CaCO_3$ precipitation and the cementation mechanism *via* SEM imaging.

Cementation Mechanism implied by microscopic analysis

Figures 7(a,b) are typical SEM images for post-treatment artificial silica sand (spherical) where the particles are uniformly encapsulated in a calcium carbonate shell. Point contact bonds develop as $CaCO_3$ shells grow in thickness and overlap with neighboring shells. This probably results from an initial uniform adhesion of the microorganisms on the sand particle surfaces and thus promotes uniform precipitation of calcium carbonate. The distributions of $CaCO_3$ precipitation on the surfaces of both near-spherical sand (Figures 7(c,d)) and angular sand (Figures 7(e,f)) are similar. The sand surfaces are covered by patchy $CaCO_3$ precipitations.

The reason why the microscopic distribution of $CaCO_3$ precipitation on spherical silica sand is quite distinct from the other two types of sands is that the bacterial used in this study (*Sporosarcina Pasteurii*) is a rod-shaped microorganism. The shape of the bacteria significantly affects its adhesion to surfaces with different roughness. Rod-shaped bacteria have a larger contact area and binding energy when contacting a smooth surface, which results in a stronger adhesion (Song et al. 2021; Whitehead et al. 2006). As a rod-shaped bacterium, *Sporosarcina pasteurii* can adhere to the smooth surfaces of spherical silica sand more firmly, thus producing uniform precipitation of calcium carbonates, resulting in larger $CaCO_3$ contents than the other two types of sands. The schematic diagram for the attachment of rod-shaped bacteria to the rough surface and smooth surface is shown in Figure 8.

Although treated artificial silica sands (spherical) features larger $CaCO_3$ content developing a uniform $CaCO_3$ coating on the sand grains, the inter-particle contact area is vanishingly small as point contacts. This results in a much smaller bonding area, implying weak bonding strength. The highlight in Figure 7(a) shows typical clean surfaces of treated

Table 2. $CaCO_3$ contents of the samples.

Particle type	Injected volume of nutrient solution(ml)/MICP-grouting cycles	$CaCO_3$ contents (%)			
		18–25 Mesh	25–40 Mesh	40–60 Mesh	60–80 Mesh
Artificial silica sand (spherical)	600/6	13.0	15.9	16.7	16.1
	800/8	17.8	20.7	21.5	23.9
	1000/10	22.3	24.5	26.4	27.3
Ottawa sand (near-spherical)	600/6	7.9	6.6	7.3	8.6
	800/8	9.2	11.3	10.4	11.8
	1000/10	13.8	14.4	15.2	15.7
Crushed Ottawa sand (angular)	600/6	6.9	7.1	7.9	7.5
	800/8	9.7	10.1	10.8	11.2
	1000/10	13.3	14.7	14.1	16.3

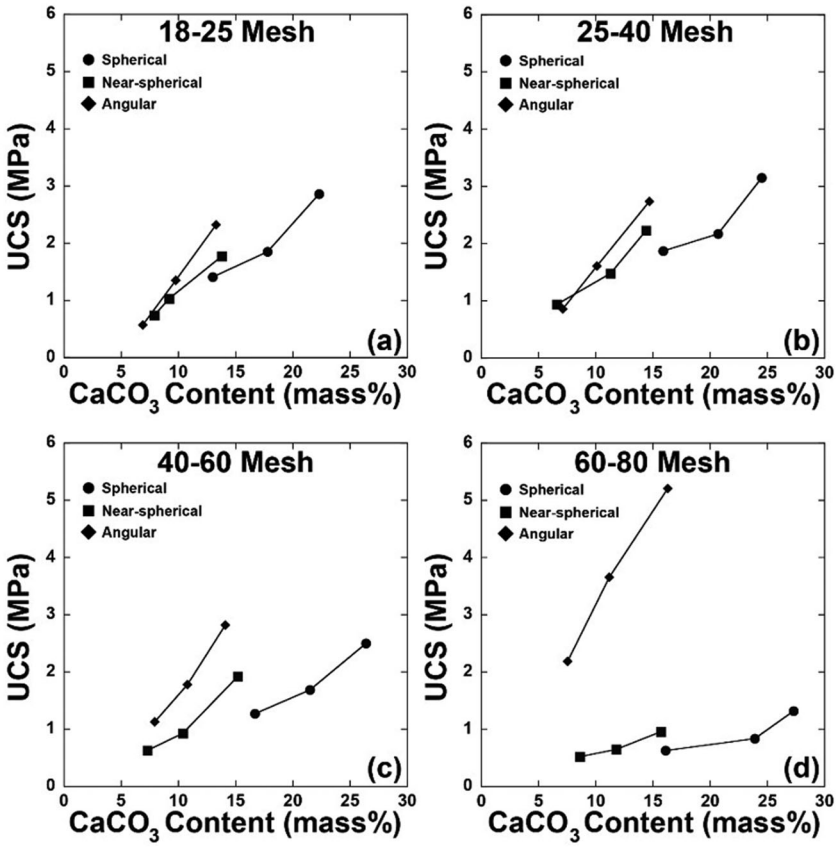

Figure 6. Correspondence between $CaCO_3$ content and UCS. The $CaCO_3$ mass content data points (3 for one type) of each type of sand corresponds to the grouting cycle of 6, 8, and 10 (injected nutrient volume of 600, 800, and 1000 ml) from left to right, respectively.

artificial silica sand plausibly caused by bond breakage, indicating weak cohesion of the $CaCO_3$ precipitation on the sand grains. For treated Ottawa sand (near-spherical) and crushed Ottawa sand (angular), the inter-particle contacts appear to feature a mix of $CaCO_3$ cemented point contacts and planar contacts, with increasing portions of the latter type. As shown in Figures 7(e,f), the crushed Ottawa sand features mostly planar contacts due to the angular geometry of the particles. These planar contact bonds provide a larger cementation area between particles and thus result in higher bonding strength. This explains why treated crushed Ottawa sands (angular) feature higher UCS with less $CaCO_3$ content than treated artificial silica sands (spherical).

In a bonded assembly, ensemble strength can be related to the size of bonds between grains. In a point-contact-bond-dominated assembly, for example, artificial silica sand (spherical), the bond size does not increase as the particle size increases. Larger grains mean greater moment on the point contact bonds under stress, which results in reduced ensemble UCS as the particle size increase. This is the possible reason why the ensemble strength of spherical and near-spherical silica sands decreases when particle sizes surpass 25–40 mesh, as shown in Figures 5(d,e).

Conclusions

We explore the ensemble UCS of MICP treated silica sands with spherical, near-spherical, and angular grain shapes and for different grain sizes. The influence of various MICP-grouting cycles on post-treatment UCS is examined. Post-treatment, $CaCO_3$ contents are measured, and SEM imaging analysis is performed to explore the distribution of the cementation, and thus to reconcile mechanisms contributing to the difference in strength gains across different samples.

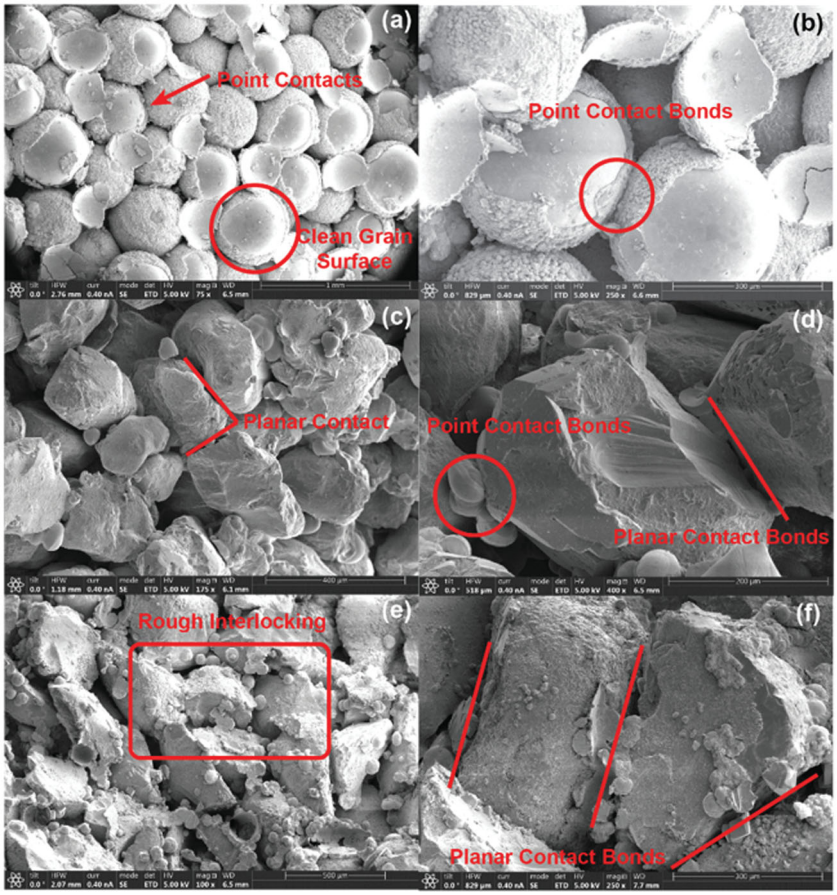

Figure 7. The SEM image of (a,b) treated artificial silica sand (spherical), (c,d) treated Ottawa sand (near-spherical), (e,f) treated crushed Ottawa sand (angular). Images correspond to 40–60 mesh samples with six cycles of MICP-grouting on each particle shape category; other samples show similar features.

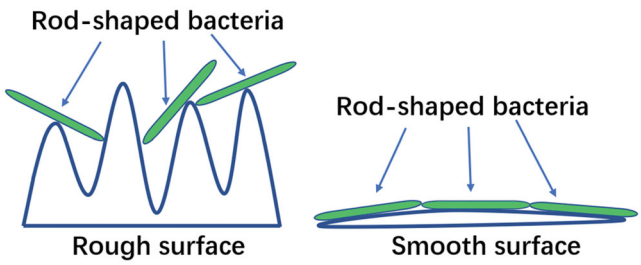

Figure 8. Schematic diagram representing the attachment of rod-shaped bacteria to the rough surface and smooth surface.

Particle morphology is shown to exert critical control on the degree and form of cementation, and subsequentially on UCS. The following conclusions are drawn:

a. MICP-treated crushed Ottawa sand (angular) shows increasing UCS with decreasing particle size.
b. Given injected nutrient volume, MICP-treated artificial silica sand (spherical) and Ottawa sand (near-spherical) attain the largest UCS at a particle size of 25–40 mesh, with larger particle sizes reducing the ensemble UCS.
c. The ensemble strength of the treated aggregate does not depend solely on calcium carbonate content—the microstructure of the cementation and the form of bonds, namely, point bonds and planar bonds, exert a controlling influence.

Particle morphology and resultant bonding mechanisms exert critical controls in MICP-grouting that significantly affect the cementation structure and, as a result, the ensemble strength of the treated assemblage.

Acknowledgments

The authors are grateful for this support.

Disclosure statement

No potential conflict of interest was reported by the author(s).

Funding

The financial support from the National Natural Science Foundation of China (Grant No. 51604051), the Key Laboratory of Hydraulic and Waterway Engineering of the Ministry of Education (Project No. SLK2021B04), and the State Key Laboratory Cultivation Base for Gas Geology and Gas Control (Project No. WS2020A02).

References

Al Qabany A, Soga K, Santamarina C. 2012. Factors affecting efficiency of microbially induced calcite precipitation. J Geotech Geoenviron Eng 138(8):992–1001.

Cardoso R, Pedreira R, Duarte SOD, Monteiro GA. 2020. About calcium carbonate precipitation on sand biocementation. Eng Geol 271:105612.

Choi SG, Hoang T, Park SS. 2019. Undrained behavior of microbially induced calcite precipitated sand with polyvinyl alcohol fiber. Appl Sci 9(6):1214.

DeJong JT, Fritzges MB, Nüsslein K. 2006. Microbially induced cementation to control sand response to undrained shear. J Geotech Geoenviron Eng 132(11):1381–1392.

Imseeh WH, Alshibli KA, Moslehy A, Kenesei P, Sharma H. 2020. Influence of crystal structure on constitutive anisotropy of silica sand at particle-scale. Comput Geotech 126:103718.

Liu B, Zhu C, Tang CS, Xie YH, Yin LY, Cheng Q, Shi B. 2020. Bioremediation of desiccation cracking in clayey soils through microbially induced calcite precipitation (MICP). Eng Geol 264:105389.

Mahawish A, Bouazza A, Gates WP. 2018. Effect of particle size distribution on the bio-cementation of coarse aggregates. Acta Geotech 13(4):1019–1025.

Mortensen BM, Dejong JT. 2011. Strength and Stiffness of MICP Treated Sand Subjected to Various Stress Paths. Geotechnical Special Publication.

Mortensen BM, Haber MJ, Dejong JT, Caslake LF, Nelson DC. 2011. Effects of environmental factors on microbial induced calcium carbonate precipitation. J Appl Microbiol 111(2):338–349.

Nafisi A, Khoubani A, Montoya BM, Evans MT. 2018. The effect of grain size and shape on mechanical behavior of MICP sand I: Experimental study. Proceedings of International Symposium on Bio-mediated and Bio-Inspired Geotechnics, p1–9.

Peng J, Liu Z. 2019. Influence of temperature on microbially induced calcium carbonate precipitation for soil treatment. PLOS One 14(6): e0218396.

Salifu E, MacLachlan E, Iyer KR, Knapp CW, Tarantino A. 2016. Application of microbially induced calcite precipitation in erosion mitigation and stabilisation of sandy soil foreshore slopes: A preliminary investigation. Eng Geol. 201:96–105.

Song C, Chen Y, Wang J. 2020. Plugging high-permeability zones of oil reservoirs by microbially mediated calcium carbonate precipitation. ACS Omega 5:14376–14383.

Song C, Elsworth D. 2018. Strengthening mylonitized soft-coal reservoirs by microbial mineralization. Int J Coal Geol. 200:166–172.

Song C, Elsworth D. 2020. Microbially induced calcium carbonate plugging for enhanced oil recovery. Geofluids 2020:1–10.

Song C, Elsworth D, Zhi S, Wang C. 2021. The influence of particle morphology on microbially induced $CaCO_3$ clogging in granular media. Mar Georesources Geotechnol. 39(1):74–81.

Song C, Liu S. 2020. A novel approach of bulk strength enhancement through microbially-mediated carbonate cementation for mylonitic coal. Geomicrobiol J. 37(8):726–737.

Ulusoy U, Kursun I. 2011. Comparison of different 2D image analysis measurement techniques for the shape of talc particles produced by different media milling. Miner Eng. 24(2):91–97.

Wen K, Li L, Zhang R, Li Y, Amini F. 2019. Micro-scale analysis of microbial-induced calcite precipitation in sandy soil through SEM/FIB imaging. Micros Today. 27(1):24–29.

Whitehead KA, Rogers D, Colligon J, Wright C, Verran J. 2006. Use of the atomic force microscope to determine the effect of substratum surface topography on the ease of bacterial removal. Colloids Surfaces B Biointerfaces. 51(1):44–53.

Wu C, Chu J, Wu S, Hong Y. 2019. 3D characterization of microbially induced carbonate precipitation in rock fracture and the resulted permeability reduction. Eng Geol 249:23–30.